AIP | Review of Scientific Instruments

Thermal characterization and analysis of microliter liquid volumes using the three-omega method

Shilpi Roy-Panzer, Takashi Kodama, Srilakshmi Lingamneni, Matthew A. Panzer, Mehdi Asheghi, and Kenneth E. Goodson

Citation: Review of Scientific Instruments **86**, 024901 (2015); doi: 10.1063/1.4907353
View online: http://dx.doi.org/10.1063/1.4907353
View Table of Contents: http://scitation.aip.org/content/aip/journal/rsi/86/2?ver=pdfcov
Published by the AIP Publishing

Thermal characterization and analysis of microliter liquid volumes using the three-omega method

Shilpi Roy-Panzer,[1,a)] Takashi Kodama,[2] Srilakshmi Lingamneni,[2] Matthew A. Panzer,[2] Mehdi Asheghi,[2] and Kenneth E. Goodson[2]
[1]*Department of Electrical Engineering, Stanford University, Stanford, California 94305, USA*
[2]*Department of Mechanical Engineering, Stanford University, Stanford, California 94305, USA*

(Received 21 October 2014; accepted 19 January 2015; published online 11 February 2015)

Thermal phenomena in many biological systems offer an alternative detection opportunity for quantifying relevant sample properties. While there is substantial prior work on thermal characterization methods for fluids, the push in the biology and biomedical research communities towards analysis of reduced sample volumes drives a need to extend and scale these techniques to these volumes of interest, which can be below 100 pl. This work applies the 3ω technique to measure the temperature-dependent thermal conductivity and heat capacity of de-ionized water, silicone oil, and salt buffer solution droplets from 24 to 80 °C. Heater geometries range in length from 200 to 700 μm and in width from 2 to 5 μm to accommodate the size restrictions imposed by small volume droplets. We use these devices to measure droplet volumes of 2 μl and demonstrate the potential to extend this technique down to pl droplet volumes based on an analysis of the thermally probed volume. Sensitivity and uncertainty analyses provide guidance for relevant design variables for characterizing properties of interest by investigating the tradeoffs between measurement frequency regime, device geometry, and substrate material. Experimental results show that we can extract thermal conductivity and heat capacity with these sample volumes to within less than 1% of thermal properties reported in the literature. [http://dx.doi.org/10.1063/1.4907353]

I. INTRODUCTION

The biology and biomedical communities continue to improve instrumentation for polymerase chain reaction (PCR) and related DNA diagnostics and processing techniques. These improvements are enabling reductions in samples volumes. However, continuing to scale current detection approaches is challenging, and thermal based detection methods may provide promising alternatives. For example, DNA genotyping and melt curve characterization are conventionally performed using fluorescent detection methods that require the use of fluorescent probes or intercalating dyes. However, the reliance on the binding of probes to the product for detection imposes additional measurement uncertainty.[1] Furthermore, detection of small fluorescence signals becomes technically difficult due to low signals when working with the 100 pl volumes and low concentrations to which current PCR technology is striving. Thus, alternatives based on thermometry, such as calorimetry,[2] are being explored as possible means of detection in order to accommodate steadily decreasing sample volumes without the need for fluorescent probes or dyes, which can adversely influence results. Before exploring the applications of thermometry techniques to DNA and other biological samples, these techniques must be extended and validated for known fluids with the target volume of interest.

There has been extensive research on the characterization of the thermal conductivity and heat capacity of bulk fluids using several methods. Examples include the transient hot-wire technique,[3,4] calorimetry,[5–9] and the 3ω method, which have been applied to sample volumes of tens of microliters (μl) and, more recently, to volumes down to the picoliter (pl) and to the nanoliter (nl) range using nanostructured heater devices.[10–18] A major challenge with the reduction of sample volume is reduced signal. Even when the sample size is large, the confined depth of interrogation made possible by the 3ω method can strongly reduce the effective sample volume. The size of the heater used is a critical factor affecting the minimum probed volume, as the heater must be entirely surrounded by the fluid. In several studies that reported values of fluid thermal properties using the 3ω method, those that utilized suspended wires used wire lengths of at least 8 mm, limiting the minimum feasible sample volume.[13,14,16] Various on-substrate 3ω devices characterized fluid thermal properties with heaters that ranged from 1 mm to 6 mm in length,[10,12] while several groups used smaller microfabricated heaters to apply 3ω to sub-μl volumes.[11,15,18] However, there has been little investigation of the boundary of the thermal volume probed and limitations on detection sensitivity.

The 3ω measurement is typically sensitive to both the thermal conductivity and heat capacity of the sample when working with small volumes. Thus, in biological samples where both of these properties are typically unknown, the data analysis often needs to extract both of these parameters simultaneously. A number of previous studies have reported values of both thermal conductivity and heat capacity. However, to our knowledge, none of these have presented a thorough uncertainty analysis and investigation for the 3ω technique to determine the accuracy of multi-parameter fits and the impact of design parameters of the experiment. The

a)Author to whom correspondence should be addressed. Electronic mail: shilpir@stanford.edu.

present work addresses the need to accurately characterize the thermal properties of biologically relevant fluids while investigating the sensitivity and uncertainty limits of extending and scaling this detection technique to the much smaller volumes of interest. Additionally, since many biological and phase change material applications are strongly temperature-dependent, demonstrating that 3ω can readily characterize the temperature-dependent thermal properties of μl volumes over required temperature ranges is a necessary step towards such applications. While some of the previous studies characterized room-temperature thermal conductivity and heat capacity of μl volume scale fluids, few of these studies reported the temperature-dependence of these properties.[13] Thus, in addition to validating the method, data for the temperature dependence of the thermal properties of fluids relevant for biological applications are required.

Here, we first present a detailed analysis of the thermal probed volume of the heaters designed in this work as compared to those in other literature. This thermal volume analysis explores the feasibility of extending this technique to pl volume detection. Second, this work presents much needed uncertainty and sensitivity analyses of the 3ω method when applied to small volumes. A sensitivity analysis determines the effect of varying heater aspect ratios, geometry, and substrate materials on the sensitivity of detection of both thermal conductivity κ and volumetric heat capacity C_p as a function of frequency. This analysis provides guidance about the best measurement frequency regime for a device of specific dimension and substrate material to characterize the parameter of interest. The sensitivity capabilities of the measurement tools developed here, along with the ability to measure micro-to-picoliter volumes, demonstrate the potential of the 3ω method for biological processes and other applications where detection of very small thermal perturbations in the system is necessary. The uncertainty analysis investigates the efficacy of the least-squares fitting algorithm used to extract κ and C_p of the fluid sample to determine the error in the fitted parameters. We discuss several trade-offs between volume, sensitivity, and operational frequency regime in these 3ω measurements. Applying these techniques, we measure the temperature-dependent thermal properties of μl volumes of common biological liquids including samples of de-ionized (DI) water, a salt buffer solution comprised of tris buffer and $MgCl_2$ (commonly used for bio-applications), and a 1cSt silicone oil to experimentally determine their temperature-dependent thermal conductivity and heat capacity from room temperature (24 °C) to 80 °C. We demonstrate the accuracy of this technique when applied to μl samples by comparing these values of thermal conductivity κ and volumetric heat capacity C_p to available literature values.

II. EXPERIMENT

The measurement devices consist of metal heaters fabricated on a fused silica substrate using e-beam evaporation of a 5 nm thick titanium adhesion layer and 60 nm thick platinum layer, patterned using lift-off photolithography. The heater design targets the highest measurement sensitivity considering photolithography resolution limits (2 μm minimum feature size) and the target length below 1 mm for μl droplet volumes. Since a 2 μl DI water droplet on a substrate has an approximate diameter of 2 mm, we ensure the entire heater is contained under the fluid volume by restricting the heater lengths to a range of 200 μm–700 μm. To maintain high aspect ratio, heater widths range from 2 μm to 5 μm. The shorter heater lengths facilitate the study of smaller droplets, while the higher aspect ratio heaters maximize the sensitivity of the measurement. Figure 1 shows the layout of each device, containing two isolated heater lines separated by a 100 μm gap. Following the metal patterning, a 45 nm silicon dioxide passivation layer is deposited using an atomic layer deposition (ALD) process in order to prevent current leakage through the fluid, which is particularly significant for conductive sample measurements. The conformal nature of the ALD technique ensures a high-quality thin passivation film to electrically isolate the metal heaters from electrically conductive samples, without compromising thermal sensitivity. The oxide thickness is determined using an ellipsometer after fabrication. To provide access to the metal contact pads, a second photolithography step is utilized to selectively etch the oxide from the contact pads. Droplets of the liquid are then placed via pipet directly on top of the heater structures.

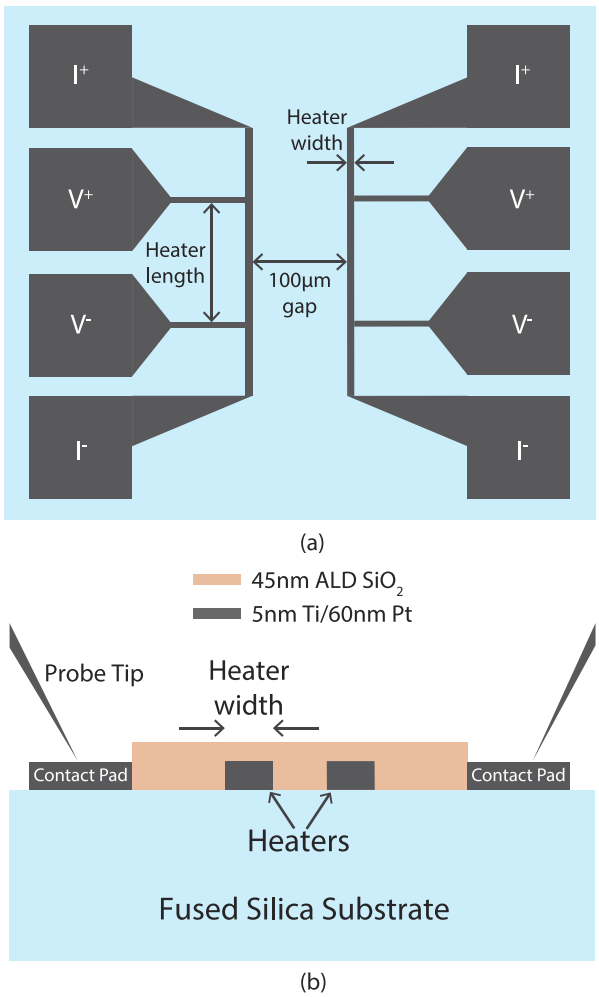

FIG. 1. (a) Top view of two isolated heater lines. (b) Cross-sectional view of device with 45 nm ALD SiO_2 passivation layer etched away from metal contact pads to provide probe tip access.

The 3ω measurement drives an AC current through a metal heater at frequency ω, which results in Joule heating and subsequent temperature oscillation in the heater line at frequency 2ω. The 3ω voltage captures the average temperature rise occurring in the heater, which is governed by the thermal properties of the surrounding materials, and can be used to extract κ and C_p of fluids. Using the solution for thermal diffusion through stratified media with a modulated heating source at an arbitrary point,[19,20] the average temperature rise ΔT seen at the heater can be derived as

$$\Delta T = \frac{P}{2\pi L b^2}\int_0^\infty \frac{B^+(m)+B^-(m)}{A^+(m)B^-(m)-A^-(m)B^+(m)} \times \frac{\sin^2(mb)}{\gamma_j m^2}dm, \tag{1a}$$

$$\gamma_j = \kappa_j\sqrt{m^2 - i\frac{\omega}{D_j}}, \tag{1b}$$

where P, L, and b are the heating power, length, and half-width of the heater line, respectively. The parameters κ_j and D_j correspond to the thermal conductivity and diffusivity of layer j, m is the variable of integration, and $B^+(m)$, $B^-(m)$, $A^+(m)$, and $A^-(m)$ are dimensionless parameters solved by a recursive matrix method.[19,20] A least squares algorithm fits the experimental 3ω data to the analytical solution, Eq. (1), to extract the unknown parameters (thermal properties or heater geometry). Further technical details of the thermal analysis and implementation of the 3ω method are extensively discussed in prior literature.[21–23] In the present work, the temperature-dependent 3ω measurements are carried out in the frequency range of 200 Hz–6 kHz. The minimum thermal diffusion length at the highest frequency (HF) is significantly longer than the thickness of the 45 nm oxide film. Conversely, both the sample volume and fused silica substrate boundaries are semi-infinite in comparison to the approximate maximum thermal penetration depth of 27 μm from the heater for the lowest frequency (LF). This frequency range is chosen to probe smaller fluid volumes by reducing the frequency-dependent radial thermal penetration depth to the order of tens of microns. An initial 3ω measurement on the bare fabricated devices verifies the measurement rig and characterizes the heater width and thermal properties of the fused silica substrate by fitting the experimental calibration data for the heater half-width, b, and κ and C_p of the substrate simultaneously. Due to the narrow widths of the heater lines in this study, it is essential to characterize any deviance from the nominal heater width (due to lift-off effects), as this will affect the resistance of the heater and the subsequent temperature rise and 3ω signal.

Droplets of volume 2 μl are used for the measurement of DI water and salt buffer solution, while a bulk volume of 15 μl is used for silicone oil. These respective volumes are chosen based on the rate of evaporation at elevated temperatures during the temperature-dependent measurement. To prevent evaporation of the DI water and salt buffer solutions, 20 μl of mineral oil is placed on top of the droplets; however, as the silicone oil sample used is very low viscosity (1cSt), it does not share the same segregated properties with water or other oils, so a larger bulk volume must be measured to preserve the sample during the duration of measurement. To contain the fluid, an acrylic well of dimensions 3.5 mm × 3.5 mm × 5 mm (height) is fixed to the substrate using a thin layer of epoxy. The μl volumes of fluid sample are placed on the oxide surface via pipetting, such that the droplet covers the entire heater length, which is imperative for temperature and material property uniformity along the heater line. A heater of dimensions 700 μm length and 4 μm width is used for all three fluids.

III. RESULTS AND DISCUSSION

A. Probed volume analysis

Although bulk fluid volumes down to 2 μl are used for all samples in this work, the transiently heated volume is significantly smaller and defined by the heater geometry and the frequency-dependent thermal penetration length into the fluid. Since the minimum required sample volume is related to the thermally probed volume, to discuss extending the 3ω method to samples of smaller volumes, we first define the thermally probed volume as

$$V_t = \int_V dV\frac{\Delta T(\vec{r})}{\Delta T(0)}, \tag{2}$$

where $\Delta T(0)$ is the average temperature at the heater surface at $(x,y) = (0,0)$ and $\Delta T(\vec{r})$ represents the average temperature at a given radial vector $\vec{r}$ into the medium. Since the radius of the thermally probed volume as calculated using Eq. (2) is below that of the physical droplet boundary, we are insensitive to the conditions of the droplet boundary in this work.

The dependence of the thermal volume probed on heater dimensions and measurement frequency can be understood through limiting cases of the analytical solution to Eq. (2). In the low-frequency limit, due to the quasi-steady-state conditions of the 3ω measurement, heat diffusion is limited by lateral spreading from the heater and dictated significantly by the heater width dimension. Thus, the thermal penetration has low sensitivity to heating time scales, and consequently a low sensitivity to heat capacity. In this low-frequency regime, Eq. (2) reduces to a measured volume approximated by the half-volume of a cylinder, $V_{LF} = 0.5\pi(l_{heater})(r_{2Dpen}{}^2)$, where l_{heater} is the heater length, and r_{2Dpen} is the radial penetration depth. The quantity r_{2Dpen} is derived from the analytical solution at $x = 0$ and defined as the radial depth at which the temperature drops to $(1/e)\Delta T$, where ΔT is the average temperature change at the heater surface. Accounting for radial spreading effects, this penetration depth is calculated at $x = 0$ using the expression

$$\Delta T(\vec{r}) = \int_{-b}^{b}\frac{P}{l\pi\kappa}\cdot \mathrm{K}_0\left(q\sqrt{(x-x')^2+y^2}\right)dx'. \tag{3}$$

Equation (3) is derived from the radial solution for an infinitely thin heater.[21,24] The thermal penetration at $x = 0$ (at the center of the heater) is found by integrating along the width of the heater, where b is the half-width of the heater, P/l is the power per unit length generated by the line heater, and κ is the thermal conductivity of the semi-infinite layer (using properties of DI water in these simulations). The parameter K_0 is the 0th order Bessel function of the quantity qr, or $q\sqrt{x^2+y^2}$, where q is

the complex thermal wave number defined as

$$q = \sqrt{\frac{i2\omega\rho c_p}{\kappa}}, \tag{4}$$

where ρ, c_p, and κ are the density, specific heat, and thermal conductivity of the semi-infinite layer, respectively, and ω is the angular frequency of the driving current.[12]

Conversely, at the high-frequency limit, the heat diffusion equation reduces to one-dimensional thermal propagation, with the thermal penetration depth dictated by $r_{1Dpen} = \sqrt{2\,\alpha/\omega}$, where α is the thermal diffusivity of the fluid. In this regime, the thermal penetration depth into the fluid is smaller than the heater half-width. Thus, Eq. (2) reduces to a probed volume given by the product of the heater length, the full heater width, and the one-dimensional thermal penetration depth ($V_{HF} = l_{heater} \times w_{heater} \times r_{1Dpen}$).

Figure 2 illustrates the thermally probed volume over the frequency range in this work by numerically evaluating Eq. (2) and the resulting volume for the smallest designed heater of width 2 μm and length 200 μm. Figure 2 compares the volume probed in this work to others in the literature which uses traditional 3ω to analyze fluid thermal properties. Other groups who have performed small volume measurements using 3ω cite larger bulk volumes as their minimum sample size. However, the same analysis of probed volume was performed on the 3ω measurements in the works shown in Fig. 2, using their smallest feasible heater geometries and the extreme limits of their specified frequency ranges and is included in Fig. 2 for comparison. For all numerical integration, a spatial domain of 3 times the penetration depth is used for both the x and y coordinates for each frequency.

The heaters in this work offer the unique opportunity to work in both the high and low frequency regimes while requiring a maximum volume of 10 nl. This flexibility in frequency of heating while consistently probing such small volumes is very useful for many biological applications, where reaction kinetic time scales can vary dramatically and sample sizes are traditionally small.

B. Sensitivity and uncertainty analyses

One of the challenges of extending measurement techniques down to small volume regimes is maintaining measurement accuracy and sensitivity comparable to those in larger volume samples. Previous work, while briefly discussing the ability of 3ω to independently determine κ or C_p in different frequency regimes,[12,16,25] has not engaged in detailed studies of sensitivity. Most 3ω measurements conducted on microliter and sub-microliter volume samples are restricted in part by the width and length of the heaters themselves while attempting to maintain aspect ratios that enable high measurement sensitivity. Measurement sensitivity is largely controlled by this heater aspect ratio, where a larger length to width ratio allows for great signal-to-noise detection capability by decreasing the dT/dR of the heater. Since the temperature oscillations at the surface of the heater can be calculated from the expression[21]

$$\Delta T = 2\frac{V_{3\omega}}{I}\frac{dT}{dR}, \tag{5}$$

minimizing the value of dT/dR will maximize the 3ω voltage signal, thus reducing the minimum detectable change in heater temperature, ΔT_{min}, which is ultimately determined by the measurement system. The sensitivity analysis shown in Fig. 3 examines the sensitivity capabilities of heaters with varying aspect ratios, including those used in this work. We perform this analysis by perturbing the thermal property of interest, either κ or C_p of the fluid above the heater, to calculate the corresponding change in the signal ΔT. The sensitivity coefficients for both κ and C_p, are defined as

$$S_\kappa = \frac{\partial \ln(\Delta T)}{\partial \ln(\kappa)} = \frac{\Delta(\Delta T)/\Delta T}{\Delta\kappa/\kappa};$$
$$S_{C_p} = \frac{\partial \ln(\Delta T)}{\partial \ln(C_p)} = \frac{\Delta(\Delta T)/\Delta T}{\Delta C_p/C_p}, \tag{6}$$

and are computed accordingly. Figure 3 illustrates the frequency-dependent sensitivity coefficients for both κ and C_p for a range of 1 mHz–100 kHz for typical heater widths.

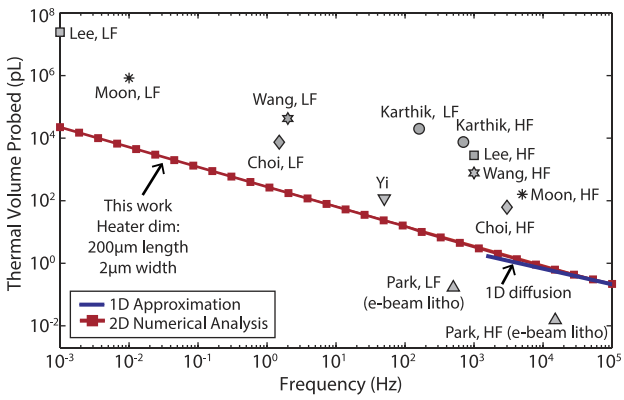

FIG. 2. Red line with squares: A 2D numerical analysis of the volume probed for the smallest heater (200 μm length, 2 μm width) used in this work. Blue line: 1D diffusion approximation. Black points of various shapes: Comparison of the liquid volumes examined by previously published papers, calculated using the same method in this paper from their reported heater geometries and measurement frequency range from LF to HF.

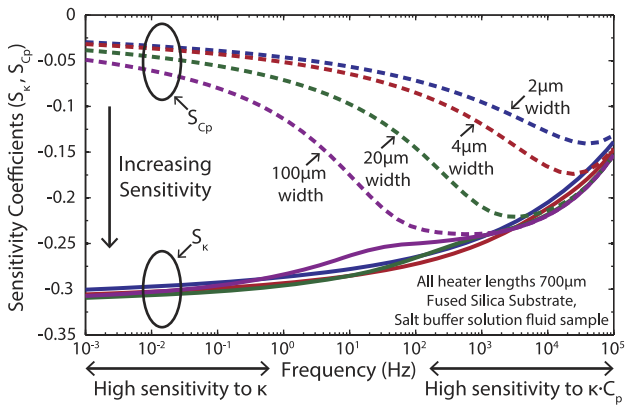

FIG. 3. A sensitivity analysis with salt buffer fluid sample, exploring low to high frequency regimes, illustrates the frequency-dependent sensitivity coefficients for both κ and C_p for a range of 1 mHz–100 kHz, using heaters of 700 μm length and widths of 2 μm, 4 μm, 20 μm, and 100 μm. The curves for both S_κ and S_{C_p} converge as the solution approaches the 1D limit and the measurement is dominated by the sample effusivity.

For each frequency point, the change in ΔT is analytically determined for a defined change in κ or C_p of the sample, after which the sensitivity coefficient is calculated using Eq. (6). Figure 3 shows sensitivity coefficients for heaters of length 700 μm and different widths, including the most sensitive heater in this work (2 μm width), the heater used for these temperature-dependent measurements (4 μm width), and other hypothetical heater geometries for comparison (20 μm and 100 μm widths). In the analysis, we use the measured room-temperature thermal properties of the salt buffer solution and fused silica substrate. The sensitivity curves illustrate that the amplitude of the 3ω signal applied is dominated by κ in the low frequency regime, while it is governed by the product of κ and C_p, or the sample effusivity shown in Eq. (7),

$$e = (\kappa C_p)^{1/2}, \tag{7}$$

at higher frequencies in the 1D heat diffusion regime. These differing sensitivities over the frequency range provide the opportunity to independently characterize κ and C_p. As the heater width increases, the effect of 1D diffusion begins to influence measurements at lower frequencies. Eventually, with relatively wide heaters and consequently low aspect ratios, it becomes increasingly difficult to resolve κ or C_p independently, as a significant portion of the frequency regime is only sensitive to the sample effusivity.

Figure 4 depicts the minimum changes in κ and C_p that are capable of being detected given the system and heater design parameters used in this work. These minimum thresholds are determined by evaluating the percent change in each parameter while fixing the other parameter that generates the minimum detectable heater temperature variation, ΔT_{min}. ΔT_{min} is evaluated by considering both the experimental and system noise contributions, where the experimental noise is attributed to uncertainty in the measurement of dT/dR, and the system noise is due to the inherent noise floor of the system equipment. To correctly characterize the value and variation of dT/dR, which is an empirically determined, intrinsic characteristic of the heater line, multiple temperature vs. resistance curves is taken with the measurement heater at both low and high driving currents.[21] In the low frequency regime, the noise is dominated by this frequency-independent uncertainty in the frequency-independent dT/dR. Due to the frequency dependence of the amplitude of the 3ω signal, this leads to a frequency-dependent noise in ΔT. At the high frequency limit, the relative contribution of dT/dR is minimal, and the noise of the system equipment begins to dominate due to the low 3ω signal levels. Using a time constant of 300 ms on the lock-in amplifier, we take the system noise to be equivalent to the measured 3ω signal standard deviation ($N \geq 5$). To calculate ΔT_{min} for a hypothetical heater geometry, we take the square root of the sum of squares of each noise contribution to ΔT_{min}. To compute the dT/dR component of ΔT_{min}, in this theoretical investigation, we assume the limits of sensitivity are given by holding the maximum current density constant at the value used in this work, j_{max}. We also hold constant the intensive heater metal properties of electrical resistivity ρ_e and temperature coefficient of resistance α, as well as heater length l and cross-sectional area A. Using these parameters, we calculate the average power output from the heater and use Eq. (5) to compute the theoretical 3ω voltage, $V_{3\omega}$, where ΔT is found using Eq. (3) and includes a thermal transfer function, Z, which is a function of parameters b, κ, C_p, and ω. We then use the value of $V_{3\omega}$ in Eq. (5), using the percent uncertainty in dT/dR, represented by $\%X$, α, ρ_e, and the heater geometry. For the system noise component of ΔT_{min}, we use the standard deviation of the 3ω voltage, $V_{3\omega,stdev}$, in Eq. (5). Taking both components into account, we can express ΔT_{min} as

$$\Delta T_{min} = \sqrt{\left(2\cdot\frac{V_{3\omega}}{j_{max}\cdot A}\cdot\frac{1}{\alpha\cdot\rho_e\frac{l}{A}}\cdot\%X\right)^2 + \left(2\cdot\frac{V_{3\omega,stdev}}{j_{max}\cdot A}\cdot\frac{1}{\alpha\cdot\rho_e\frac{l}{A}}\right)^2}, \tag{8a}$$

where

$$V_{3\omega} = \frac{{j_{max}}^3\cdot{\rho_e}^2\cdot\alpha\cdot l\cdot A\cdot Z(b,\kappa,C_p,\omega)}{2}. \tag{8b}$$

We apply this analysis to the heater of highest sensitivity in this work, with 700 μm length and 2 μm width, as well as heaters of different aspect ratios, keeping the length constant and using widths of 4 μm, 20 μm, and 100 μm, and using a fused silica substrate and salt buffer fluid sample. Results, shown by the solid curves in Fig. 4, use a dT/dR uncertainty of 0.5% and $V_{3\omega,stdev}$ of ±1 μV. Though the solid curves indicate comparable sensitivity to κ for all heater aspect ratios, we observe that smaller changes in C_p can be resolved with decreasing aspect ratio. This conclusion is due to our initial assumption of maintaining constant maximum current density across all heater geometries, which leads to an increase in output power for lower aspect ratio heaters. This initial assumption may pose an issue at low frequencies for small aspect ratio heaters with large power outputs due to the resulting large temperature oscillation at the heater surface. When performing temperature-dependent measurements, large temperature perturbations at the heater surface in the range of tens of kelvin may introduce nonlinearities in the heat equation and subsequent thermal properties. Thus, this assumption of constant maximum current density presents an extreme trend which may only be experimentally viable in the high frequency regime where temperature oscillations decay to more reasonable amplitudes.

To pose a more limiting assumption, we next fix the maximum temperature oscillation at the surface of the heater at the lowest frequency of 1 mHz, using the maximum ΔT of our highest aspect ratio heater (700 μm length by 2 μm width). Using this calculated current density in place of j_{max} in Eq. (8), we observe the reverse sensitivity trend overall, indicated by the dashed curves in Fig. 4. Depending on the application of interest, the minimum necessary volume, and the resulting frequency of operation, the appropriate aspect ratio and heater geometry can be chosen using this analysis.

An additional analysis is performed to demonstrate the effect of substrate material on the measurement sensitivity. Sensitivity coefficients for κ and C_p are determined according to Eq. (6) while varying the substrate materials and geometry to investigate methods of further optimizing sensitivity while maintaining the small volume regime of this measurement.

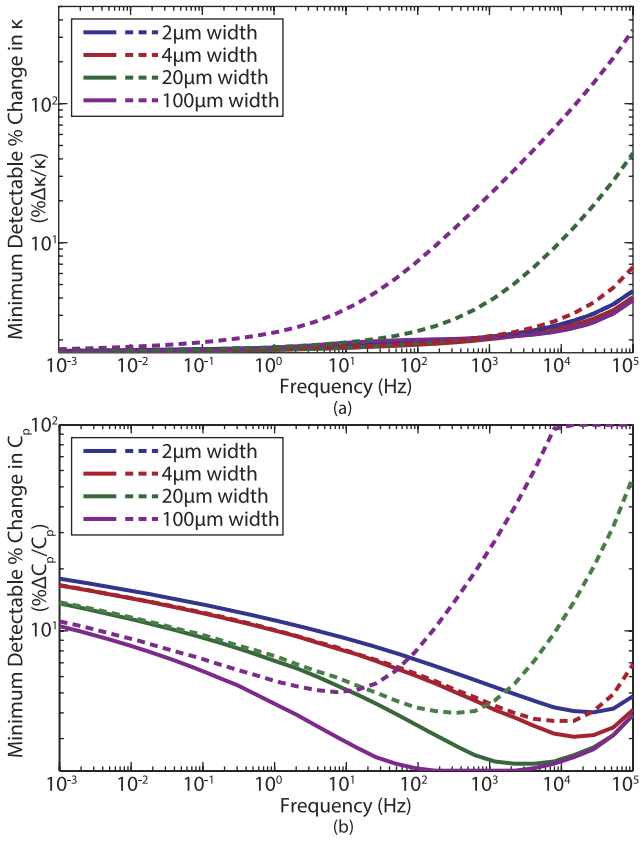

FIG. 4. Minimum detectable changes in (a) κ and (b) C_p based on frequency-dependent error in ΔT_{min} from a range of 1 mHz to 100 kHz, using a heaters of 700 μm length and widths of 2 μm, 4 μm, 20 μm, and 100 μm. Analysis uses a fused silica substrate and salt buffer fluid sample. ΔT_{min} found using analysis explained in Eq. (7). Solid curves assume constant current density across all heater geometries. Dashed curves assume maximum temperature oscillation at the heater surface at the lowest frequency of 1 mHz.

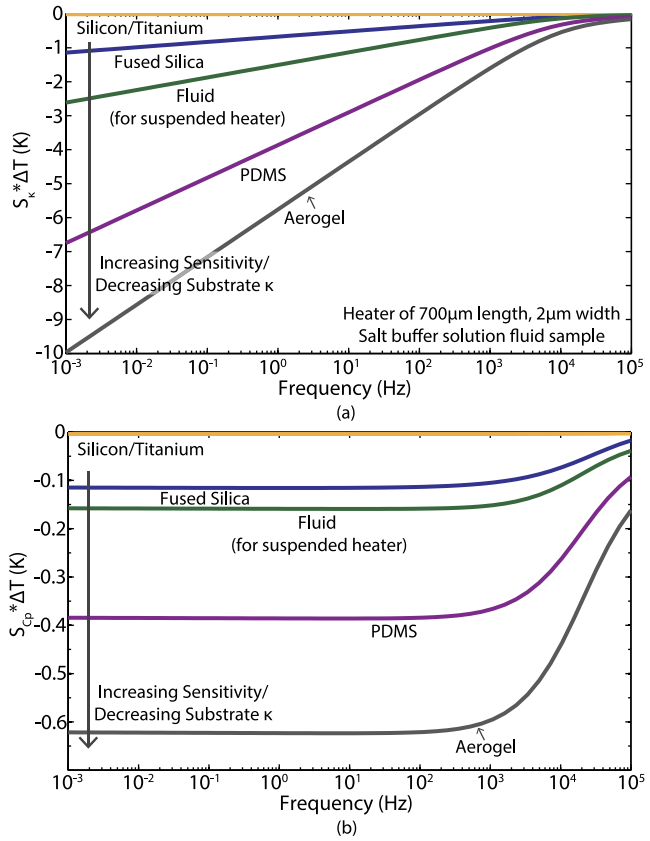

FIG. 5. Sensitivity analysis to demonstrate the effect of substrate material on both the sensitivity coefficients for (a) thermal conductivity κ and (b) volumetric heat capacity C_p, coupled with the magnitude of temperature oscillation of the heater for a frequency range of 1 mHz–100 kHz. In addition to the fused silica substrate used in this work, we investigated substrate materials including silicon (κ = 149 W/m K^{-1}, C_p = 1.66 MJ/m^3 K^{-1}), titanium (κ = 21.9 W/m K^{-1}, C_p = 2.35 MJ/m^3 K^{-1}), surrounding sample fluid (by means of a suspended heater structure, salt buffer solution κ = 0.625 W/m K^{-1}, C_p = 3.53 MJ/m^3 K^{-1}), PDMS (κ = 0.15 W/m K^{-1}, C_p = 1.42 MJ/m^3 K^{-1}), and silica aerogel (κ = 0.017 W/m K^{-1}, C_p = 840 J/m^3 K^{-1}).[26] Curves indicate increasing sensitivities to both κ and C_p with decreasing substrate thermal conductivity. Analysis performed with a heater of 700 μm length and 2 μm width and salt buffer fluid sample.

In addition to the fused silica substrate used in this work, the analysis explores alternative substrate materials such as silicon, titanium, polydimethylsiloxane (PDMS), and silica aerogel. Finally, a suspended heater structure is investigated, in which the fluid sample surrounds the heater and acts as the substrate. Figure 5 illustrates the sensitivity results of all of these geometries for a frequency range of 1 mHz–100 kHz for a heater of 700 μm length and 2 μm width. Using a more thermally insulating substrate material such as PDMS or silica aerogel, where substrate thermal conductivity is orders of magnitudes less than that of silicon dioxide, results in increased heat conduction through the fluid sample above. Thus, detection of even smaller changes in κ and C_p is feasible. Conversely, with highly conductive materials such as silicon and titanium, the substrate acts like a heat sink, drastically reducing the magnitude of temperature oscillation at the heater, the subsequent 3ω signal, and the resulting ability to resolve significant changes in κ and C_p. To capture these effects, the sensitivity coefficients of both κ and C_p are multiplied by the magnitude of temperature oscillation of the heater, ΔT. This product compensates for the effect of the substrate material on the magnitude of the 3ω signal, as well as the measurement sensitivity. Figure 5 shows this product of S_κ and S_{C_p} with the respective ΔT oscillations of the heater as a function of frequency. The analysis has assumed the following nominal values for each substrate material: silicon (κ = 149 W/m K^{-1}, C_p = 1.66 MJ/m^3 K^{-1}), titanium (κ = 21.9 W/m K^{-1}, C_p = 2.35 MJ/m^3 K^{-1}), surrounding fluid (salt buffer solution of κ = 0.625 W/m K^{-1}, C_p = 3.53 MJ/m^3 K^{-1}), PDMS (κ = 0.15 W/m K^{-1}, C_p = 1.42 MJ/m^3 K^{-1}), and silica aerogel (κ = 0.017 W/m K^{-1}, C_p = 840 J/m^3 K^{-1}).[26]

An uncertainty analysis is performed to quantify the limitations of the least squares algorithm to fit uniquely for both κ and C_p, which dominates the uncertainty in the temperature-dependent results. To understand the contributions to uncertainty, we quantify the ability to fit uniquely by observing how well the analytical solution fits the data. The uncertainty analysis accomplishes this by shifting and fixing one parameter (either κ or C_p), indicated on the x-axis, while fitting freely for the second parameter, which is indicated on the right-side y-axis. We then evaluate the rms error of the deviation between the experimental data and analytical

solutions, which is plotted on the left-side y-axis. This rms error, or η, is calculated using the expression

$$\eta = \frac{\Delta\epsilon}{\epsilon} = \sqrt{\frac{\sum_{i=1}^{N}\left(\frac{T_{experimental,i}-T_{analytical,i}}{T_{analytical,i}}\right)^2}{N}}, \qquad (9)$$

where N is the number of frequency points, and $T_{experiemental,i}$ and $T_{analytical,i}$ are the experimental and analytical temperature profiles, respectively. Figure 6 investigates this uncertainty using 3ω data taken for DI water over a frequency range of 50 Hz–10 kHz, shifting and fixing κ and fitting freely for C_p in Fig. 6(a), and shifting and fixing C_p and fitting freely for κ in Fig. 6(b). In addition, the analytical fits for several different frequency sub-ranges are considered to understand the impact of frequency range choice on measurement certainty. Within the wider frequency spectrum, we include the ranges of 50 Hz–2 kHz, 3.2–5.6 kHz, and 4 kHz–10 kHz. The minimum in each uncertainty curve represents the optimal fit of the algorithm, and the corresponding κ and C_p values at that minimum are taken as the measured sample properties. If the fit is highly unique, we expect the error to deviate strongly as soon as we move away from the optimal parameter values. In Fig. 6(a), the width of the valley corresponds to the relative percent uncertainty in the value of κ, within which it is difficult to establish a truly unique fit without prior knowledge of the value of C_p. If we look at the DI water data set over the largest frequency range of 50 Hz–10 kHz, shown by the solid blue curve in Fig. 6(a), where a 0% change in κ corresponds to the literature thermal conductivity for bulk DI water, we see a unique minimum at this nominal value for κ. The solid black curve in Fig. 6(a) shows the resulting, freely fit C_p for that value of κ, which also corresponds to the nominal literature value for C_p. Similar effects are observed for the reverse parameters in Fig. 6(b).

The dotted red curves in Figs. 6(a) and 6(b) show the fitting ability for a narrower frequency range of 50 Hz–2 kHz. We observe a unique minimum in κ in Fig. 6(a), but a wider valley in the minimum of C_p in Fig. 6(b), which indicates an inability to resolve a unique heat capacity, supporting our prior sensitivity analysis. There is a slight negative shift in the minimum value of κ, indicating that the algorithm will characterize the thermal conductivity as a value of 4% less than the nominal κ of DI water. Conversely, in the high frequency regimes, indicated by the dashed green curve (4 kHz-10 kHz) and dotted-dashed pink curve (3.2 kHz-5.6 kHz), we observe flatter, wider curves in both parameters. These flat curves correspond to low sensitivity to resolving either parameter independently, which confirms our prior analysis of being unable to fit uniquely for both parameters at higher frequencies, validating our sensitivity to only the sample effusivity. Additionally, for the high frequency range of 4 kHz-10 kHz, the lack of curvature of the ΔT vs. 2ω curve makes it difficult for the least-squares algorithm to fit either value appropriately, as the 3ω voltage and corresponding ΔT signal have a weaker dependence on frequency in high frequency regimes. There are opposing trends in deviation from the nominal values of κ and C_p, with a positive error in κ corresponding to a negative error in C_p, supporting an overall sensitivity to the sample effusivity.

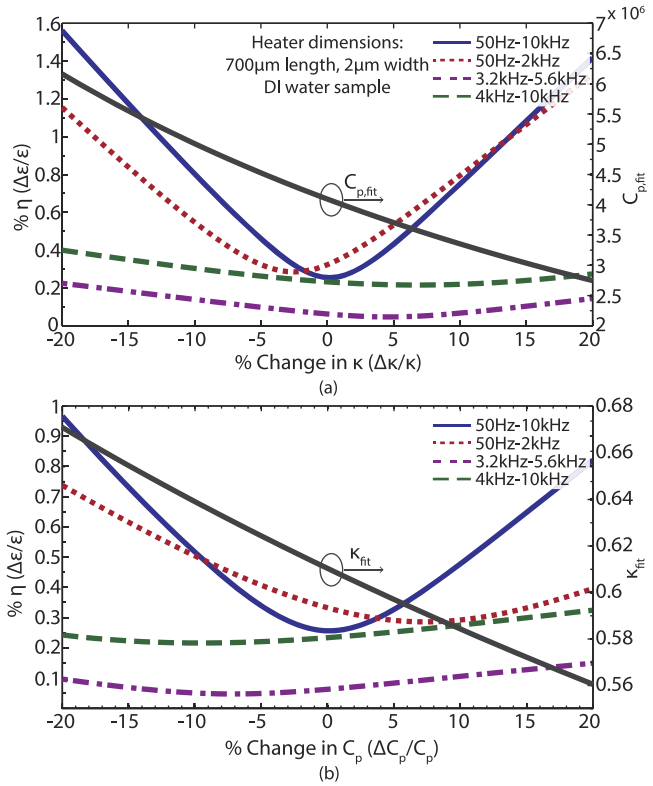

FIG. 6. Uncertainty analysis performed with least squares fitting algorithm for both κ and C_p in various frequency ranges. Analysis uses heater dimensions of 700 μm length and 2 μm width, a DI water sample, and fused silica substrate. Percent deviation of (a) κ and (b) C_p, respectively, is held constant while optimizing for the second parameter, shown on the right side y-axis for the widest frequency range; the percentage fitting error is reported using the deviation in the normalized sum of the squared temperature residuals. The minima and corresponding parameters represent the "best fit" by the algorithm, where the widest frequency range provides values closest to the literature values of DI water. Flatter and wider curves indicate low sensitivity to resolving that parameter independently, with higher deviation in the minimum fit parameter value.

There is a compromise between volume, sensitivity, and operational frequency regime in these 3ω measurements. Devices can accommodate smaller volumes while maintaining sensitivity by implementing narrow heaters and high heater aspect ratio, but this comes at the price of being sensitive only to κ and not to C_p. Additionally, such a design forces the measurement to higher frequency regimes to resolve the effusivity, thus lowering the overall sensitivity to C_p. In order to become more sensitive to C_p, wider heaters are more ideal but require an increased sample volume, which is often not desirable for many biological applications, where sample sizes are decreasing steadily. If a specific application constrains the measurement to a given frequency regime for the sake of resolving frequency-dependent processes, such as reaction kinetics, then other parameters such as heater width and length can be tuned to change the relative sensitivity to κ and C_p. These tradeoffs are essential to consider in optimal device design for each application. To apply these 3ω measurements to even smaller volume regimes by maintaining high aspect ratio while shrinking heater lengths and widths, we investigate the minimum detectable changes in κ and C_p for four heater geometries in Fig. 7, using a fused

silica substrate and salt buffer fluid sample. We extend the method previously explained in Eq. (8) to three smaller heater geometries with the aspect ratio of the 700 μm by 4 μm heater used in this work and maintain the maximum current density used experimentally to prevent electromigration effects. The minimum detectable changes in both thermal properties are plotted against the thermally probed volume to understand the feasible measurement limitations. Though smaller heater geometries down to 400 nm width show detectable changes in κ of 10% and less for volumes above 1 pl, sensitivity to changes in C_p falls drastically when shrinking heater dimensions down further than those proposed in this work.

C. Applications to fluids for biological applications

We now apply these analyses to measure temperature-dependent κ and C_p of three common fluid samples used in fluid and biological applications. To isolate the temperature-dependence of the fluid thermal properties, a preliminary measurement captures the thermal conductivity and volumetric heat capacity of the fused silica substrate, shown in Fig. 8. Since the thermal resistance of the 45 nm ALD SiO_2 passivation layer is over an order of magnitude lower than that of the surrounding materials during the time scales of these measurements, measurements are insensitive to variations to uncertainty in the film thermal properties and literature values are assumed. Based on the above sensitivity and uncertainty analysis, the heaters used in this work have reduced lateral dimension in order to provide independent sensitivity to κ and C_p. These limits on the uniqueness of the algorithm to simultaneously fit κ and C_p are the main source of uncertainty in individual property values. The multiple parameter fit comes at the expense of increased uncertainty in the measured values as compared to data extraction when there are fewer independent unknown variables.

Following the temperature-dependent characterization of the substrate materials, we measured bulk fluid volumes of 2 μl for DI water and the salt buffer solution, and 15 μl for silicone oil, at intermittent temperatures from 24 °C to 80 °C. The thermal properties found for the substrate materials at each temperature were used and fixed when fitting for the thermal conductivity and heat capacity to isolate the contribution of temperature-induced changes in the fluid thermal properties. Table I compares the room temperature characteristics of DI water and silicone oil to literature values. We found excellent agreement for each sample, with errors below 1% for both κ and C_p. Literature values for the salt buffer solution are not readily available.

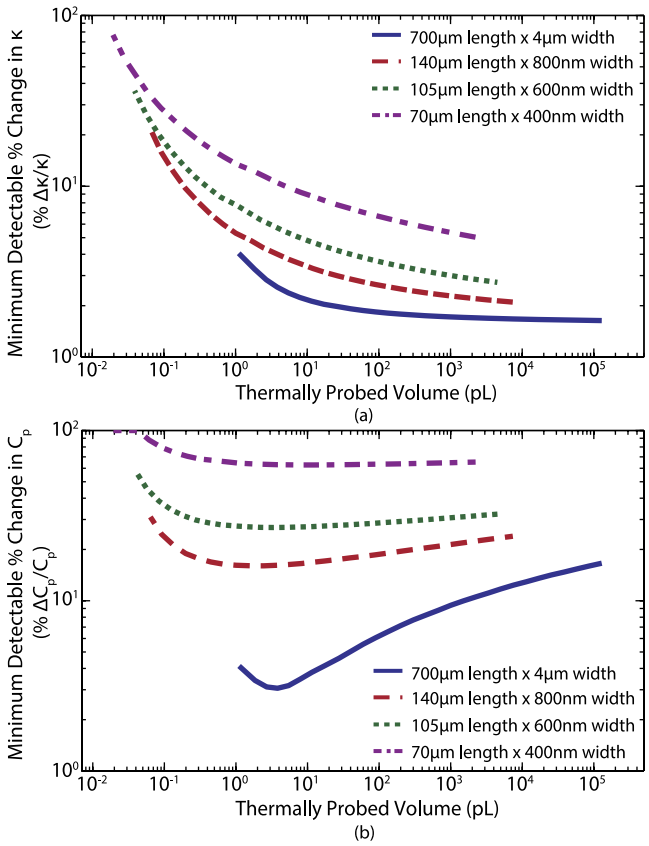

FIG. 7. Minimum detectable changes in κ (a) and C_p (b) vs. the thermally probed volume for the heater used in this work (700 μm length by 4 μm width) and three smaller heater geometries of the same aspect ratio. Analysis uses a fused silica substrate and salt buffer fluid sample. Analysis is done using method explained in Eq. (8) using constant maximum current density to prevent electromigration effects.

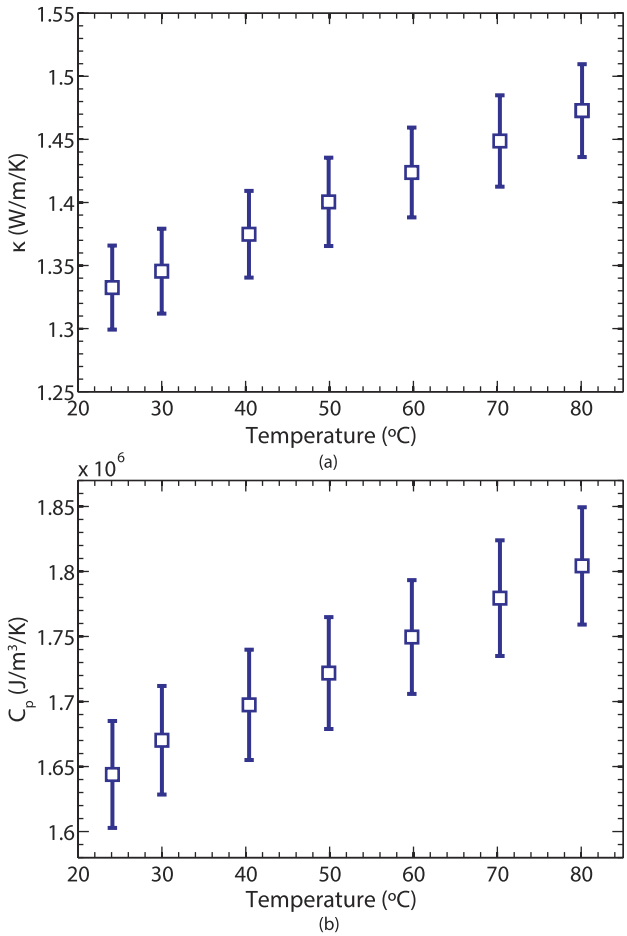

FIG. 8. Temperature-dependent thermal conductivity (a) and volumetric heat capacity (b) of the fused silica substrate. Uncertainty bars are governed by the ability of the least squares fitting algorithm to uniquely identify κ and C_p, discussed in Sec. III B.

TABLE I. Room temperature thermal properties of DI water and silicone oil compared to literature values.

Fluid	κ (W/m K^{-1}) experimental	κ (W/m K^{-1}) literature	C_p (J/m^3 K^{-1}) experimental	C_p (J/m^3 K^{-1}) literature	% error $(\%\Delta\kappa/\kappa)/(\%\Delta C_p/C_p)$
DI water	0.604	0.605[a]	4.17×10^6	4.17×10^6[a]	0.13/0.07
Silicone oil	0.099	0.1[b]	1.65×10^6	1.64×10^6[b]	0.80/0.25

[a]At 300 K, Ref. 26.
[b]At 300 K, Ref. 27.

Figure 9 illustrates the temperature-dependence of κ and C_p for DI water, salt buffer solution, and silicone oil, with comparison to the available literature values for DI water.[26] Since we were able to identify no temperature-dependent literature for this specific silicone oil (above room temperature), the trends in κ and C_p were compared to fluorinated oil, for which there is temperature-dependent literature on thermal properties. Due to their similarities in

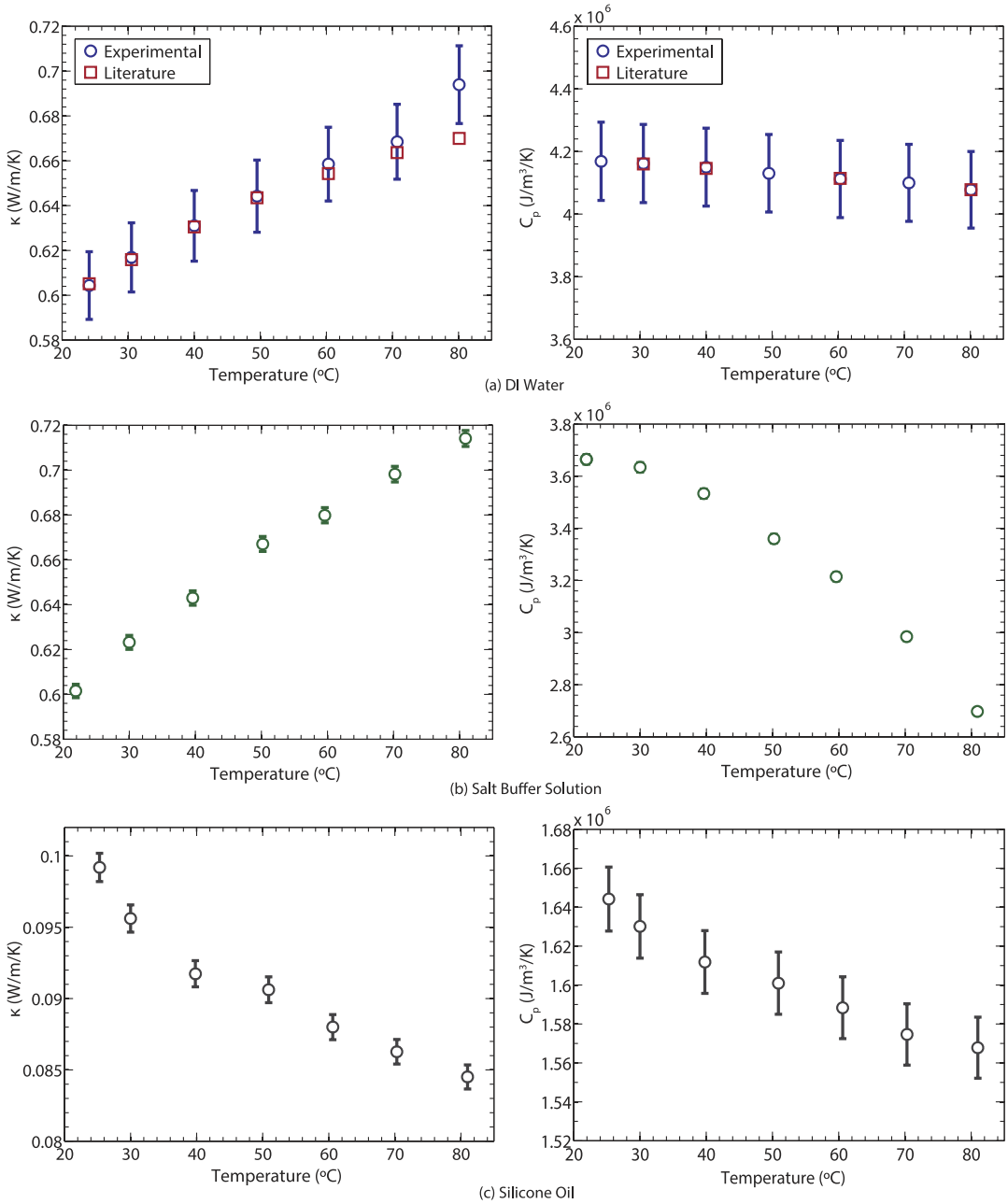

FIG. 9. Temperature-dependent thermal conductivity and volumetric heat capacity of (a) DI water, with comparison to literature values,[26] (b) salt buffer (markers partially conceal error bars), and (c) 1cSt silicone oil. Uncertainty bars are governed by the ability of the least squares fitting algorithm to uniquely identify κ and C_p, discussed in Sec. III B. All data are taken with heater of length 700 μm and width 4 μm.

viscosities and molecular weight, their temperature-dependent trends in thermal conductivity, density, and specific heat are assumed to follow closely. The thermal conductivity of the fluorinated oil was seen to decrease with increasing temperature, consistent with the trend seen for silicone oil in Fig. 9(c). The specific heat and density of fluorinated oil have opposing trends. However, the overall effect in volumetric heat capacity is dominated by the decreasing density as temperature rises, which is similar to the trend in silicone oil seen in Fig. 9(c).

IV. CONCLUDING REMARKS

In this work, we investigate the application of the 3ω method to the measurement of temperature-dependent thermal properties, κ and C_p, of small volume fluids, specifically focusing on maximizing the heater sensitivity while probing nanoliter to picoliter volumes within high and low frequency regimes. We perform detailed analyses studying sensitivity coefficients for κ and C_p, the minimum detectable changes in both parameters, as well as the substrate material effects on these sensitivity coefficients coupled with the magnitude of temperature oscillation at the heater. Depending on the heating frequency, changes in κ and C_p as small as 0.5% and 2%, respectively, can be detected with the devices in this work. An in-depth uncertainty analysis illustrates the effectiveness of the least-squares algorithm when performing a two-parameter fit, demonstrating that wider frequency ranges generally offer more unique and accurate data fitting. An analysis of thermally probed volume is performed, demonstrating the ability of our heaters to probe significantly smaller volumes than those in other works, which are forced to operate at higher frequencies in order to probe volumes of the same order. The sensitivity and small volume capabilities of the heaters in the present work suggest an opportunity for an improved detection mechanism for biological reactions in particular, where flexibility in frequency is required while minimizing volume and maximizing sensitivity. This work offers insight into the tradeoffs between volume, sensitivity, and operational frequency regime, which are essential to consider in optimal device design for each application.

ACKNOWLEDGMENTS

Acknowledgments to Tim English from Stanford University Mechanical Engineering for ALD support, and Bio-Rad Laboratories for supplying silicone oil and salt buffer samples. The authors gratefully acknowledge the financial support of the National Science Foundation Graduate Research Fellowship, as well as the Semiconductor Research Corporation (SRC) through task 2252.001.

[1]L. Zhou *et al.*, Clin. Chem. **51**, 1770 (2005).
[2]T. V. Chalikian, J. Volker, G. E. Plum, and K. J. Breslauer, Proc. Natl. Acad. Sci. U. S. A. **96**, 7853 (1999).
[3]H. M. Roder, J. Res. Natl. Bur. Stand. **86**, 457 (1981).
[4]Y. Nagasaka and A. Nagashima, Rev. Sci. Instrum. **52**, 229 (1981).
[5]J.-L. Garden, E. Château, and J. Chaussy, Appl. Phys. Lett. **84**, 3597 (2004).
[6]W. Lee *et al.*, Proc. Natl. Acad. Sci. U. S. A. **106**, 15225 (2009).
[7]Y. Zhang and S. Tadigadapa, Appl. Phys. Lett. **86**, 034101 (2005).
[8]J. Lerchner *et al.*, Thermochim. Acta **477**, 48 (2008).
[9]E. A. Johannessen *et al.*, Appl. Phys. Lett. **80**, 2029 (2002).
[10]S. R. Choi, J. Kim, and D. Kim, Rev. Sci. Instrum. **78**, 084902 (2007).
[11]S. R. Choi and D. Kim, Rev. Sci. Instrum. **79**, 064901 (2008).
[12]I. K. Moon, Y. H. Jeong, and S. I. Kwun, Rev. Sci. Instrum. **67**, 29 (1996).
[13]R. Karthik *et al.*, J. Eng. Thermophys. **21**, 60 (2012).
[14]S.-M. Lee, Rev. Sci. Instrum. **80**, 024901 (2009).
[15]B. K. Park *et al.*, Rev. Sci. Instrum. **83**, 106102 (2012).
[16]Z. L. Wang *et al.*, Int. J. Thermophys. **28**, 1255 (2007).
[17]S. N. Schiffres and J. A. Malen, Rev. Sci. Instrum. **82**, 064903 (2011).
[18]N. Yi *et al.*, Lab Chip **11**, 2378 (2011).
[19]A. Feldman, NISTIR 5928 (1996); HighTemp. High-Pressures **31**, 293 (1999).
[20]J. H. Kim, A. Feldman, and D. Novotny, J. Appl. Phys. **86**, 3959 (1999).
[21]D. G. Cahill, Rev. Sci. Instrum. **61**, 802 (1990).
[22]C. Dames and G. Chen, Rev. Sci. Instrum. **76**, 124902 (2005).
[23]M. L. Bauer and P. M. Norris, Rev. Sci. Instrum. **85**, 064903 (2014).
[24]H. S. Carslaw and J. C. Jaeger, *Conduction of Heat in Solids* (Oxford University Press, Oxford, 1959), p. 193.
[25]L. Lu, W. Yi, and D. L. Zhang, Rev. Sci. Instrum. **72**, 2996 (2001).
[26]Thermophysical Properties of Matter, Center for Information and Numerical Data Analysis and Synthesis, Purdue University.
[27]Shin-Etsu Silicone Fluid, DM-FLUID, Performance Test Results, Shin-Etsu Chemical Co., Ltd.